# Inverse problem in avalanche dynamics models

C. Ancey, M. Meunier, and D. Richard

Research Unit Torrential Erosion, Snow and Avalanches, Domaine Universitaire, Saint-Martin-d'Hères, France

Received 2 October 2002; accepted 20 December 2002; published 22 April 2003.

[1] Avalanche dynamics models are increasingly used to estimate the features of extremely rare events for avalanche zoning. They employ a frictional coefficient, which reflects something close to snow viscosity. As this coefficient is more conceptual than physical, it cannot be measured and must be fitted by matching avalanche dynamics model results and field data. However, most of the time, the historical record is not long enough to fit this coefficient for extremely rare events. Here we propose a deterministic inversion method to obtain the probability density function of this coefficient. The method has been applied to two avalanche paths in the French Alps, each with a sustained avalanche activity over the last century. For applications the Voellmy avalanche dynamics model has been used with no loss of generality. It is shown that the friction coefficient is a random variable whose marginal probability distribution varies rapidly and exhibits two or more peaks. *INDEX TERMS:* 1863 Hydrology: Snow and ice (1827); 3210 Mathematical Geophysics: Modeling; 3260 Mathematical Geophysics: Inverse theory; *KEYWORDS:* avalanche, inverse problem, Tikhonov regularization, conceptual model

**Citation:** Ancey, C., M. Meunier, and D. Richard, Inverse problem in avalanche dynamics models, *Water Resour. Res.*, *39*(4), 1099, doi:10.1029/2002WR001749, 2003.

## 1. Introduction

[2] The catastrophic avalanches of winter 1999 in Europe (Montroc, France, 12 deaths; Evolène, Switzerland, 12 deaths; Galtür, Austria, 39 deaths) have renewed the interest in developing scientific methods for avalanche zoning. Basically, an engineer in charge of avalanche zoning at a given site wishes to estimate the avalanche deposit boundaries and potential impact pressure for different periods of return [*Mears*, 1992; *Hopf*, 1998]. Two classes of tools are currently available but they are far from being satisfactory in engineering and zoning applications.

[3] Deterministic models reduce avalanche physics to a set of equations of motion, usually involving mass and momentum balance equations [*Hopfinger*, 1983; *Hutter*, 1996; *Ancey*, 2001]. The main criticism made of the current deterministic models is that they use *ad hoc* assumptions on the rheological behavior of snow [*McClung and Schaerer*, 1993]. Despite various attempts to find physical justifications for their expressions [see, e.g., *Salm*, 1993], the constitutive relationships used so far remain speculative and empirical. Given the severe difficulties faced with snow rheometry, the physical calibration of constitutive parameters used in these models will remain unfeasible for a long time. An alternative approach to fitting parameters involves comparing the model outputs and field data such as the velocity at a given point and the point of furthest reach (runout distance) [see, e.g., *Schaerer*, 1974; *Buser and Frutiger*, 1980; *Dent and Lang*, 1980]. The resulting fitted values have been proposed as default values in engineering guidelines (e.g., Swiss guidelines on the so-called Voellmy-Salm-Gubler method [*Salm et al.*, 1990] or the USGS handbook [*Mears*, 1992]). Although practitioners are generally confident of these values, recent studies have pointed out weaknesses in the values proposed by the current guidelines. For instance, when comparing the predictions of various deterministic models and field data on five European sites, *Barbolini et al.* [2000] have found that the friction parameter values could be very different from the default values. Another shortcoming when applying these models to avalanche zoning is that they do not include the notion of period of return.

[4] In the black box approach, no explicit attempt is made to capture the physics of avalanches. The basic idea stems from the pioneering work of *Lied and Bakkehøi* [1980]: assuming a regional homogeneity in avalanche behavior for a given mountain range, they pooled the data from various paths in a common database. In this way, using regression techniques, they obtained the relationship between the runout distances and a number of key variables of the path profile. This methodology has been applied to different mountain ranges throughout the world [see *Bakkehøi et al.*, 1983; *McClung and Lied*, 1987; *Fujizawa et al.*, 1993] and extended to introduce the period of return as a parameter of the problem [*McClung*, 2000, 2001]. In Alpine countries, where most of the time the avalanche paths of the same mountain range exhibit no similarity in their shape, the fundamental assumption of avalanche homogeneity on a regional scale is doubtful [*Ghali*, 1996]. A major drawback of this approach is that it depends a great deal on the quantity and quality of available data. Since most of the time the only available information is the runout distance, this approach is unable to provide estimates of the potential impact pressure. Moreover, in many cases, the historical record of runout distances is not long enough and the resulting fitted probability distribution must be extrapolated to evaluate the runout distance of a long return period avalanche. However, extrapolation is far from easy and proper due to the nonsmoothness of the distribution (M. Meunier et al., Proba-


0043-1397/03/2002WR001749$09.00

bilistic predetermination of avalanche runout distances, submitted to the *Journal of Glaciology*, 2002).

[5] In-between these two classic approaches has emerged a new class of models that can be referred to as conceptual models [*Barbolini et al.*, 2000; *Barbolini and Savi*, 2001; *Bozhinskiy et al.*, 2001; *Harbitz et al.*, 2001]. They can be viewed as the combination of different modules (or submodels) describing the different processes occurring from snowfalls to avalanche deposition. Due to the large complexity in the elementary processes and their interplay, this combination is nothing but an idealized mathematical description of the steps believed to be crucial in the release and course of avalanches. In order to mimic the avalanche activity over long periods, conceptual models are based on Monte Carlo simulations and, at least, two submodels: one to quantify the occurrence of avalanche release and another to compute the avalanche motion and deposition. Though they erase some of the intrinsic disadvantages of fully deterministic and statistical approaches, they must still cope with a difficult problem: the calibration of (conceptual) parameters using the scarce physical data available. For instance, due to the lack of long series of data, *Barbolini and Savi* [2001] collected data from several paths to deduce the probability density functions of the two parameters involved in their propagation submodel; therefore the same criticism as the one pointed out above for statistical models arises: the resulting probability density functions reflect more the spatial variability of the friction coefficients from one path to another than the variability with time at a given site.

[6] In all these approaches, model calibration is needed but, surprisingly enough, little attention has been given to providing correct estimates of the model parameters without depending too much on assumptions such as regionalization. This article presents a preliminary investigation into the determination of the probability distribution of random input parameters used in conceptual models. The method proposed here enters the more general class of techniques for solving inverse problems. Here the originality lies in the fact that we need not use the physical observable variables to calibrate the model but their probability density function. In this respect, the method lies midway between deterministic techniques used for inverse problems and probabilistic search methods (e.g., Bayesian inference). If a formal relationship between the probability density functions of conceptual and observable variables can be established, then the model can be easily calibrated. In this way, even short series of field data can be used insofar as it is possible to properly define their probability density function.

[7] We begin by presenting a typical conceptual model. Various combinations have been explored by different authors [see, e.g., *Keylock et al.*, 1999; *Barbolini and Savi*, 2001; *Bozhinskiy et al.*, 2001; *Chernouss and Fedorenko*, 2001; *Harbitz et al.*, 2001; *Keylock and Barbolini*, 2001]. Here, to favor clarity and rapid understanding, we will present the simplest conceptual framework, without claiming generality and completeness. Then we will specify two methods for adjusting parameters used in the submodel devoted to avalanche motion. The methods will then be applied to two case studies. We will use the Voellmy avalanche dynamics model as the submodel of avalanche propagation; naturally the method can be extended to other avalanche dynamics models without loss of generality provided they can be inserted into the conceptual framework described in section 2. Since the Voellmy model is a rough description of avalanche dynamics and, as it stands, it suffers from unavoidable criticisms as regards its reliability, the expediency of its use will be discussed. Two case studies in the French Alps will also be presented.

## 2. A Minimalist Conceptual Framework

### 2.1. Structure of the Model

[8] In order to simulate avalanche activity along a given path over a long period of time, we are looking for a simple conceptual model with a minimum number of steps (submodels). The structure of the model is conditioned by the number and nature of the measurable physical data at hand. These usually include the avalanche runout distance (or elevation) of past events and the meteorological conditions (snowfall, wind, air temperature, etc.) recorded in a location close to the avalanche path over a sufficiently long time (several decades). The runout distance can be viewed as the response of the studied system and an output of the model while the meteorological conditions are basically input parameters of the model. A minimalist conceptual model includes two modules (see Figure 1).

[9] 1. The first module describes what happens up to the avalanche release. The avalanche release is largely conditioned by the meteorological conditions during the previous days, especially the amount of new snow [*McClung and Schaerer*, 1993; *Ancey*, 1996]. For many sites, the key meteorological parameter explaining an avalanche activity is the sum of the amount of snow fallen during the previous three days $C_{3d}$. Not all the sustained snowfalls give rise to avalanche. Thus for a given snowfall $C_{3d}$, one has to specify the probability of observing an avalanche release $p(\text{release}|C_{3d})$. The three-day snowfall $C_{3d}$ and the lag between two snowfalls $\tau$ are random variables. Their probability density functions $p_C(C_{3d})$ and $p_\tau(\tau)$ can be estimated using classic hydrological methods (renewal, annual series methods, etc.). Usually, an extreme-value distribution (or Gumbel distribution [*Gumbel*, 1958]) or an exponential distribution provides good results while a Poisson law can be used to evaluate the number of snowfalls per time unit exceeding a given threshold. Evaluation of $p(\text{release}|C_{3d})$ is simply achieved using logistic regression techniques [*Hosmer and Lemeshow*, 1986].

[10] 2. The second module describes avalanche motion and deposition. Since the runout distance is not the only output variable of interest (e.g., the velocity or the impact pressure can be of interest for engineering applications), we shall use an avalanche dynamics model. This takes the form of a set of dynamical equations, basically the mass and momentum balance equations describing the time variations of dynamical variables of avalanche motion, usually the velocity $u$ and flow depth $h$. A generic expression of this equation system is: $\dot{h} = F(h, u)$ and $\dot{u} = G(h, u; \Pi)$, where the dot denotes the time derivative, $F$ and $G$ are two functions (not to be specified at this level) of $u$ and $h$ (and, possibly, of their derivatives), and $\Pi = \{\pi_1, \pi_2, \ldots\}$ a set of mechanical parameters needed in the mechanical description of motion.

[11] With these two modules, we are able to compute the runout distance $x_{stop}$ provided that the initial conditions are known and the mechanical parameters $\Pi$ are specified. This

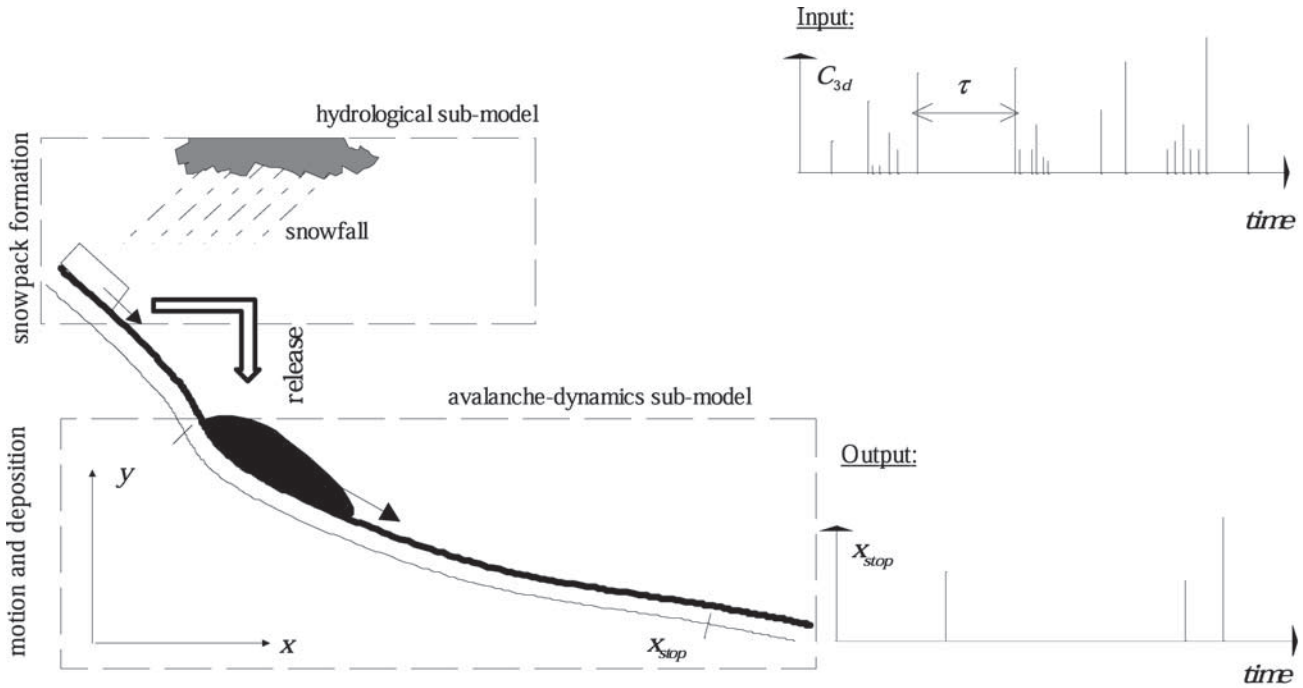


**Figure 1.** Sketch of the conceptual model used here.

also implies that there is a known dependence between the three-day snowfall and the initial conditions for the equations of motion. In the following, we express the functional dependence of the runout distance $x_{stop}$ on $\Pi$ and $C_{3d}$ as follows: $x_{stop} = Y(C_{3d}; \Pi)$.

### 2.2. Inverse Problem

[12] The basic question in the inverse problem is: given $x_{stop}$ and $C_{3d}$, what are the values of the mechanical coefficients $\Pi$? The answer is rather simple if we can invert the function $Y$ and the dimension of $\Pi$ is unity: $\pi_1 = Y^{-1}(x_{stop}; C_{3d})$. However, most avalanche dynamics models include more than one mechanical parameter. In this case, one can deduce a single mechanical parameter from the field data $x_{stop}$ provided that the other mechanical parameters are known: $\pi_1 = Y^{-1}(x_{stop}; C_{3d}|\pi_2, \pi_3, \ldots)$. Hereafter we will refer to this method as the direct method.

[13] This approach requires knowing $x_{stop}$ and $C_{3d}$ precisely for each event. This difficulty can be alleviated if we consider the problem differently. Indeed, rather than solving the equation $\pi_1 = Y^{-1}(x_{stop}; C_{3d}|\pi_2, \pi_3, \ldots)$ for each event, we can solve it globally. To be more specific, we now formulate the inversion problem in the following manner: given the probability distributions of $x_{stop}$ and $C_{3d}$, what is the probability distribution of the coefficient $\pi_1$? We will refer to this formulation as the indirect method.

[14] To answer the question above, we shall assume that the random variables $\pi_1$ and $C_{3d}$ are independent. The joint probability $p_{x,\pi}(x_{stop}, \pi_1)$ can be connected to the joint probability $p_{\pi,C}(\pi_1, C_{3d})$ by the transformation: $(x_{stop}, \pi_1) \rightarrow (C_{3d}, \pi_1)$. We denote $J_x$ the Jacobian of this transformation:

$$J_x = \left| \det \begin{bmatrix} \partial x_{stop}/\partial C_{3d} & \partial x_{stop}/\partial \pi_1 \\ \partial \pi_1/\partial C_{3d} & \partial \pi_1/\partial \pi_1 \end{bmatrix} \right| = \left| \frac{\partial x_{stop}}{\partial C_{3d}} \right| \qquad (1)$$

since $\partial \pi_1/\partial C_{3d} = 0$. Then, using the change in variables and the independence of variables $\pi_1$ and $C_{3d}$, we infer the joint probability of observing $x_{stop}$ and $C_{3d}$: $p_{x,\pi}(x_{stop}, \pi_1) = J_x^{-1} p_C(C_{3d}) p_\pi(\pi_1)$, where $p_C(C_{3d})$ and $p_\pi(\pi_1)$ denote the probability density functions of $C_{3d}$ and $\pi_1$, respectively. Thus the marginal probability density function of the runout distance is obtained by integration:

$$p_x(x_{stop}) = \int_{\mathbb{R}_+} p_{x,\pi}(x_{stop}, \pi_1) d\pi_1 = \int_{\mathbb{R}_+} J_x^{-1} p_C(C_{3d}) p_\pi(\pi_1) d\pi_1 \qquad (2)$$

If we further assume that $x_{stop} = Y(C_{3d}; \pi_1|\pi_2, \ldots)$ can be inverted to yield $C_{3d} = Y^{-1}(\pi_1; x_{stop}|\pi_2, \ldots)$, we deduce that the probability distribution $p_\pi$ satisfies a Fredholm equation of the first kind:

$$p_x(x_{stop}) = \int_{\mathbb{R}_+} K(x_{stop}, \pi_1) p_\pi(\pi_1) d\pi_1 \qquad (3)$$

where $K(x_{stop}, \pi_1) = J_x^{-1} p_C(Y^{-1}(\pi_1; x_{stop}|\pi_2, \ldots))$ is the kernel function.

[15] In practice, solving the inverse problem by the direct method is very simple since it involves finding roots to the nonlinear equation $\pi_1 - Y^{-1}(x_{stop}; C_{3d}|\pi_2, \ldots) = 0$. The indirect method requires far more work but benefits from posing the inverse problem in a probabilistic perspective. As will be illustrated below in the case studies, this formulation allows us to compute the coefficient $\pi_1$ even though we have partial series of $x_{stop}$ or $C_{3d}$. Moreover, the indirect method is especially suitable for Monte Carlo simulations, for which the values of $\pi_1$ are generated from their probability density function $p_\pi(\pi_1)$. Naturally, this method

does not suppress the parametric dependence of $\pi_1$ on the other coefficients $\pi_2$, $\pi_3$, etc.

### 2.3. Numerical Implementation of the Indirect Method

[16] The indirect method involves solving a Fredholm equation (equation 3). Here this is done numerically using the Tikhonov regularization method. We assume that the avalanche database contains $N_D$ events, whose runout distance is known. For brevity of notation, in the following we will replace $\pi_1$ by $\pi$. To begin with, we consider a mesh $\Omega$ with uniform spacing, over which $\pi$ varies. Here, we set $\Omega = [0, \pi_{\max}]$ where $\pi_{\max}$ is the maximum expected value of $\pi$. In discretized form equation (3) becomes:

$$\tilde{p}_x^C(x_i) = \zeta \sum_{j=1}^{N_K} \omega_{ij} K(x_i, \pi_j) p_\pi(\pi_j) \quad 1 \le i \le N_D \tag{4}$$

where $\pi_j$ are the $N_K$ discretization points of the interval $\Omega$, which are spaced apart by the constant step $\zeta = \pi_{\max}/N_K$: $\pi_{j+1} = \pi_j + j\zeta$, $j = 1, \ldots, N_K$ with $\pi_1 = 0$. The discretization points $\pi_j$ shall not be confused with the mechanical coefficients introduced previously and now considered as dummy variables of the kernel function. The tilde over $p_x$ indicates that the quantity is approximated; the true and the approximated quantities, respectively $p_x$ and $\tilde{p}_x^C$, differ by an amount that can be estimated on the order of $\zeta^3 \dot{p}_x$, where $\dot{p}_x$ denotes the first derivative evaluated at an unknown place in the interval $\Omega$ [*Press et al.*, 1992]. To transform the integral term into a sum, we have used a quadrature rule. For a uniform mesh, the simplest scheme is the trapezoidal rule. In this case, the quadrature coefficients are defined as follows: for a given rank $i$ ($1 \le i \le N_D$), $\omega_{1j} = 1/2$, $\omega_{ij} = 1$, $2 \le j \le N_K - 1$, $\omega_{iN_K} = 1/2$. In matrix notation, the discretized equation (4) can be written: $\tilde{\mathbf{p}}_x^C = \zeta \mathbf{W} \mathbf{p}_\pi$, where $\mathbf{W}$ is the matrix defined by $W_{ij} = \omega_{ij} K(x_i, \pi_j)$, $\tilde{\mathbf{p}}_x^C = (\tilde{p}_1, \tilde{p}_2 \ldots, \tilde{p}_{N_D})$ the set of computed values, and $\mathbf{p}_\pi = (p_1 \ldots, p_{N_K})$ the unknown vector. If we choose $N_D = N_K$ and assume that the computed values $\tilde{\mathbf{p}}_x$ coincide with the measured field data $\tilde{\mathbf{p}}_x^M = (\tilde{p}_1^M, \tilde{p}_2^M \ldots, \tilde{p}_{N_D}^M)$, we have: $\mathbf{p}_\pi = \zeta^{-1}\mathbf{W}^{-1}\tilde{\mathbf{p}}_x^C = \zeta^{-1}\mathbf{W}^{-1}\tilde{\mathbf{p}}_x^M$ and the inverse problem is easily solved. Otherwise we have $N_K$ unknown components for $N_D$ equations.

[17] The simplicity of solving a Fredholm equation is somewhat counterbalanced by the unexpected oscillations around the solution that they produce [*Baker*, 2000]. In order to reduce fluctuations of the discretized solution, it is usually better to proceed by imposing a constraint on the smoothness of the solution. A convenient method is to use Tikhonov regularization techniques [*Kirsch*, 1996]. For instance, to ensure a smooth curve, we can impose that the sum of the square of the second derivative at the discretization points, i.e.,

$$\| L_2 \mathbf{p}_\pi \|^2 = \sum_{j=1}^{N_K} \left( \frac{d^2 p_\pi}{d\pi^2}(\pi_j) \right)^2 \tag{5}$$

is minimal. In equation (5), $L_2$ is called second-order derivative operator and $\| \cdot \|$ denotes the vector norm. A finite difference estimate of the second derivative is $\ddot{p}_\pi(\pi_i) = (p_\pi(\pi_{i+1}) + p_\pi(\pi_{i-1}) - 2p_\pi(\pi_i))/\zeta^2 + o(\zeta^2)$, for $i = 2, 3, \ldots, N_K - 1$. For $i = 1$, assuming symmetry of $p_\pi$ leads to: $\ddot{p}_\pi(\pi_1) = (2p_\pi(\pi_2) - 2p_\pi(\pi_1))/\zeta^2 + o(\zeta^2)$. The boundary conditions imposed on $p_\pi$ are not too stringent because it is expected that $p_\pi \to 0$ when $\pi \to 0$ (resp. $\pi \to \pi_{\max}$). We find that the discretized form of equation (5) is:

$$\sum_{j=1}^{N_K} \left( \frac{d^2 p_\pi(\pi_j)}{d\pi^2} \right)^2 = G(\mathbf{p}_\pi) + o(\zeta^2) \tag{6}$$

where $G$ is the quadratic function $G(\mathbf{p}_\pi) = (\mathbf{B}\mathbf{p}_\pi)^{\mathrm{T}} \cdot (\mathbf{B}\mathbf{p}_\pi)$, in which $\mathbf{B}$ denotes the $N_K \times N_K$ tridiagonal matrix:

$$\mathbf{B} = \frac{1}{\zeta^2} \begin{bmatrix} -2 & 2 & 0 & \cdots & \cdots & \cdots & 0 \\ 1 & -2 & 1 & 0 & \cdots & \cdots & 0 \\ 0 & 1 & -2 & 1 & 0 & \cdots & 0 \\ \vdots & 0 & \ddots & \ddots & \ddots & 0 & \vdots \\ 0 & \cdots & 0 & 1 & -2 & 1 & 0 \\ 0 & \cdots & \cdots & 0 & 1 & -2 & 1 \\ 0 & \cdots & \cdots & \cdots & 0 & 2 & -2 \end{bmatrix} \tag{7}$$

$\mathbf{B}$ is the discretized expression of $L_2$ and therefore is called the second-order difference regularization operator. Other constraints than $L_2$ can be imposed to ensure the smoothness of the solution. For instance, instead of taking $L_2$, we can constrain the norm of the solution vector to be as low as possible to avoid overly large fluctuations. In that case, the regularization operator is the identity operator and its discretized expression is $\mathbf{B} = \mathbf{I}_{N_K}$, where $\mathbf{I}_{N_K}$ is the identity matrix of dimension $N_K$.

[18] Determining the unknown vector $\mathbf{p}_\pi$ by solving the linear system equation (4) is equivalent to finding the minimum of the functional: $F(\mathbf{p}_\pi) = \sum^{N_D} \left( \frac{\tilde{p}_x^C(x_i) - \tilde{p}_x^M(x_i)}{\tilde{p}_x^M(x_i)} \right)^2$ or in matrix form: $F(\mathbf{p}_\pi) = (\mathbf{1}_{N_D} - \mathbf{A}\mathbf{p}_\pi)^{\mathrm{T}} \cdot (\mathbf{1}_{N_D} - \mathbf{A}\mathbf{p}_\pi)$, where $A_{ij} = W_{ij}\zeta/\tilde{p}_x{}^M(x_j)$ is an $N_D \times N_K$ matrix and $\mathbf{1}_{N_D}$ is a unity vector of dimension $N_D$. If we further assume that $p_x$ defines a smooth curve, we are looking for a vector that minimizes the functional $H(\mathbf{p}_\pi) = F(\mathbf{p}_\pi) + \lambda G(\mathbf{p}_\pi)$, where $\lambda$ is a free parameter (Lagrangian multiplier). It can be shown that the solution to $\partial H(\mathbf{p}_\pi)/\partial \mathbf{p}_\pi = 0$ has a unique solution, given by [*Kirsch*, 1996]:

$$\mathbf{p}_\pi = \left( \mathbf{A}^{\mathrm{T}}\mathbf{A} + \lambda \mathbf{B}^{\mathrm{T}}\mathbf{B} \right)^{-1} \mathbf{A}^{\mathrm{T}} . \mathbf{1}_{N_D} \tag{8}$$

At this point, it should be remembered that the solution actually depends on the Lagrangian multiplier $\lambda$, which is an adjustable factor that controls the extent to which the resulting curve is smooth or close to experimental data. The functional $F$ measures something like the agreement of the solution curve to the data, while the functional $G$ reflects the "smoothness" of the curve or the "stability" relative to variations in the data. The better agreement is obtained when a "small" value of $\lambda$ is chosen, but in this case, the solution may be widely oscillating. In contrast, the best smoothness is produced when using a quite "large" value of $\lambda$. In practice, to find a good compromise between agreement and smoothness, the typical idea is to plot the

trade-off curve, i.e., $F(\mathbf{p}_\pi)$ versus $G(\mathbf{p}_\pi)$ for different values of $\lambda$ in a log linear diagram. Generally, the resulting trade-off curve is L-shaped. An appropriate value of $\lambda$ is then chosen by selecting points in the corner of the L curve [*Calvetti et al.*, 2000]. Hereafter, we will proceed differently: since the function $p_\pi$ is a probability density function, it is expected that: $\int p_\pi d\pi = 1$. Thus in the following, we generally use this condition to select an appropriate value for $\lambda$. Another property that the probability density function must fulfill is $p_\pi \geq 0$. Yet, by imposing smoothness, we may also introduce some undesirable effects such as the local negativity of the function $p_\pi$. Here, to impose $p_\pi \geq 0$, we remove all the negative values from the solution vector $\mathbf{p}_\pi$. A last remark is that an alternative more rigorous method would have been to add further constraints to the functional $H(\mathbf{p}_\pi)$ to directly take into account the two conditions $p_\pi \geq 0$ and $\int p_\pi d\pi = 1$ [e.g., see *Andreotti and Douady*, 1999]. However, because of the low number of field data, we have preferred to use the approximate method presented here. Indeed, if new constraints are added to the functional $H(\mathbf{p}_\pi)$, other parameters than $\lambda$ are also introduced. Since, to our knowledge, there are no parameter selection methods for problems with several regularization parameters, a study is needed to evaluate the sensitivity of the result when modifying the regularization parameters; the existence and unicity of the solution is not guaranteed.

## 3. Application

[19] Before applying the proposed method to real cases, we shall give a few indications on the avalanche dynamics model. Here we use a Voellmy-like model, which can be seen as a prototypal avalanche dynamics model. The model used is very close to the Voellmy-Salm-Gubler [*Salm et al.*, 1990] (VSG) model, except the approximate method of solving the equations of motion has been replaced by an ordinary differential equation, solved numerically. Since the use of avalanche dynamics models is still controversial, we will begin by explaining why we chose to use a Voellmy model. The equations and assumptions used in this model will then be presented in section 3.2. Field data have been extracted from a national database (Enquête Permanente des Avalanches), which in which information on avalanches at a large number of sites in the French Alps has been gathered for approximately one century. In section 3.3, the selected sites will be presented. Section 3.4 will address the determination of the runout function $Y$ and results will be summarized in sections 3.5–3.7.

### 3.1. Selection of an Avalanche Dynamics Model

[20] Avalanches occupy a peculiar position in geophysics in that, in contrast to lava and debris flows, there is no sound field or laboratory data available on the basic processes involved in avalanche release and flow. Therefore all the avalanche dynamics models proposed so far rely on analogy with other physical phenomena: typical examples include the analogies with granular flows [*Savage*, 1989; *Savage and Hutter*, 1989; *Tai et al.*, 2001], Newtonian fluids [*Hunt*, 1994], power law fluids [*Norem et al.*, 1986], and viscoplastic flows [*Dent and Lang*, 1982; *Ancey*, 2001]. Nonetheless, even though all these new developments appear attractive from a physical viewpoint, from a purely rheological point of view they still rely on a speculative basis. In fact, most of the time, scientists have attempted to adjust rheological parameters used in their model to a few field data (such as the leading-edge velocity and the runout distance) for their model results to be consistent with observations, but, obviously, this does not really provide evidence that the constitutive equation they used is appropriate.

[21] wIn its original formulation, the Voellmy model belongs to the class of sliding-block models, which present the advantage of leading to simple ordinary differential equations, but also the drawback of overly simplifying the physics of avalanches. Disadvantages and advantages offered by Voellmy-like models are discussed in a number of recent papers and monographs [*McClung and Mears*, 1995; *Bartelt and Gruber*, 1997; *Bartelt et al.*, 1999], to which the reader can refer. More refined models have been developed over the last two decades, notably those of *Eglit* [1983, 1984, 1998], *Bartelt and Gruber* [1997], *Bartelt et al.* [1999], and *Barbolini and Savi* [2001], and have transformed the VSG model into flow-depth averaged equations of motion (similar to shallow water equations used in hydraulics), leading to a set of hyperbolic partial differential equations.

[22] There are several reasons that led us to use a Voellmy-like model despite its limitations: (1) First of all, this model, notably in the formulation known as the Voellmy-Salm-Gubler (VSG) model, is widely used in Europe for avalanche zoning and engineering. Its success stems from this model's long history (applied in Switzerland and Russia since the 1920s, 30 years before Voellmy popularized the model) and its simplicity. The method proposed here provides the practitioner with the means to tune the model parameters from field data; this seems to us better than tabulated default values given by the guidelines. (2) Furthermore, the avalanche dynamics model is an element of the chain needed to model the physical processes from snowfall to avalanche deposition. At this stage, we are mainly interested in finding a simple mathematical model rather than a sophisticated model, which would be time-consuming and involve many parameters. Based on an ordinary differential equation and two mechanical parameters, the VSG model plainly fulfills our objective. (3) Finally, it is worth mentioning that, in our approach, the VSG model was used in a conceptual framework with the objective of mimicking avalanche activity in a given path over a long period. Thus our approach lies somewhere between purely deterministic (physically based) models and statistical (black box) models and, in this respect, is not very different from the conceptual catchment models used in hydrology. Since our primary objective is to compute the runout distance of extreme avalanches, our use of a Voellmy model appears licit; it is, however, unclear whether the method can also be applied to compute avalanche velocities and pressures with the same degree of confidence since no field data concerning these variables have been used.

### 3.2. Avalanche Dynamics Model

[23] The VSG model relies on momentum and mass balance equations for describing avalanche motion [*Salm et al.*, 1990; *Salm*, 1993]. Motion is described within the framework of rigid-body mechanics. The momentum equation is expressed as follows: $m\dot{u} = mg \sin\theta - F$, where the dot means the time derivative, $\theta$ is the path

inclination, $m$ is the avalanche mass, $u$ its velocity, and $F$ is the friction force experienced by the avalanche. For an unconfined avalanche, this force has the form: $F = \mu mg \cos\theta + mgu^2/(\xi h)$, where $h$ refers to the flow depth, $\xi$ and $\mu$ are two friction coefficients. The mass balance equation expresses that the mass flow rate $Q$ holds constant throughout the run: $Q = \rho lhu = \rho_0 l_0 h_0 u_0$, where the subscript 0 refers to the initial conditions (i.e., at the end of the release phase), $l$ denotes the avalanche width, and $\rho$ its density. Here, to simplify, we further assume that the snow density is fairly constant: $\rho \approx \rho_0$. Similarly, it is assumed that there is no significant change in the avalanche width: $l \approx l_0$.

[24] The VSG model has four input parameters: the initial conditions $h_0$ and $u_0$, and the friction parameters $\xi$ and $\mu$. It is assumed that the initial velocity (at the end of release phase) is: $u_0 = \sqrt{\xi h_0 \cos\theta_0 (\tan\theta - \mu)}$ [*Salm et al.*, 1990], where $\theta_0$ denotes the mean slope of the starting zone. The initial flow depth $h_0$ corresponds to the thickness of the released snow layer. It is assumed that this thickness is directly correlated with the amount of snow fallen during the previous three days $C_{3d}$: $h_0 = f(\theta_0) C_{3d}$, where $f(\theta_0) = 0.291/(\sin\theta_0 - 0.202\cos\theta_0)$ [*Burkard and Salm*, 1992]. The friction coefficient $\xi$ reflects the effect of path roughness. It is assumed to range from 400 to 1000 m/s$^2$ and be intrinsic to the path, that is, it is constant for each avalanche run in a given path. In contrast, $\mu$ pertains to snow fluidity. This parameter may depend on the avalanche size and/or other parameters. Its lower value given in the literature is 0.155 and corresponds to extreme avalanches [*Buser and Frutiger*, 1980]. In short, we have three effective input parameters ($\xi$, $\mu$, $C_{3d}$), two of which can be considered as random variables ($\mu$, $C_{3d}$) while the third ($\xi$) can be assumed to be constant (for a given site).

[25] We found no clear evidence in the literature for the last assumption. However, as shown in section 3.4, insofar as we are involved in working with $x_{stop}$ and we constrain $\xi$ to lie within the prescribed range of 400–1000 m/s$^2$ [*Salm et al.*, 1990], the precise determination of $\xi$ is of less importance since $x_{stop}$ usually depends weakly on $\xi$. Thus in this case, if we apply the inverse problem method to the parameter $\pi_1 = \mu$, the final parametric dependence $\mu(\xi)$ on $\pi_2 = \xi$ is found to be weak so that, as a first approximation, it is permissible to make the calculation as if $\mu$ were really independent of $\xi$. However, if one leaves the VSG framework, that is, if $\xi$ can take any real value, the direct inversion method will provide $\mu$ values depending on $\xi$ and the indirect inversion method will provide the conditional probability density function $p_\mu(\mu|\xi)$.

[26] In the following, we will remain within the spirit of the VSG method. Thus we want to determine the values of $\pi_1 = \mu$; the second coefficient $\pi_2 = \xi$ is held constant (see section 3.4).

### 3.3. Sites

[27] We have applied the two inversion methods to different sites in the French Alps. Emphasis was given to selecting avalanche sites with (1) a nearby meteorological station and (2) snow and avalanche data over a sufficiently long period. Here we present the results obtained on two sites. It will be shown that the indirect inversion method provides well-behaved results for the first site (Plan de l'Aiguille) but results only in a qualitative agreement with the second site (Bessans).

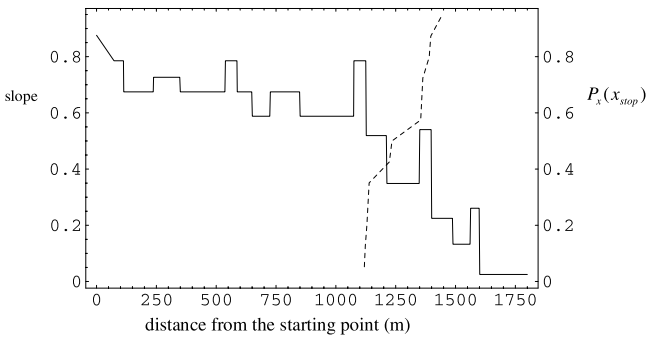


**Figure 2.** Variation in the path slope as a function of the distance from the starting point (solid line) along with the cumulative distribution function of the runout distance for the Plan de l'Aiguille site.

[28] The first site is the Plan de l'Aiguille avalanche path. It is located above Chamonix (Mont Blanc mountain range). The path extends between 2150 and 1030 m in elevation and its length exceeds 1.7 km. The path is slightly confined and its sides are covered with sparse forests. Figure 2 shows the variation in the ground slope along the path. Avalanche data have been recorded since 1901. The avalanche database includes 40 events, but the time series is not complete, notably during the two world wars, when there was no record. Uncertainty on the runout distance varies with time. At the beginning of the 20th century, it probably exceeded ±100 m while nowadays it is expected to be much lower (±20 m). Figure 2 shows the empirical cumulative probability distribution of the runout distance along with the slope of the path profile. The origin, from which the runout distance is computed, is taken from an arbitrary point in the starting zone (without loss of generality). Since only the lower part of the avalanche path (alluvial fan) can be conveniently observed from the valley, the database includes events that reached the alluvial fan, that is, those whose runout distance exceeded 1100 m. Due to the irregularity of the path slope, a number of avalanches probably stopped in the upper part of the site and were not recorded since they could not be observed.

[29] The meteorological station has been recording snow data since 1960. It is located at an elevation of 1050 m and is 2 km from the starting zone. We used the moment method to find the probability density function of three-day sums of snowfall and tested different probability distributions. The best agreement with data was obtained with an exponential distribution. We have found that the probability of observing an amount of snow fallen within three days is described by:

$$p_C(C_{3d}) = \exp\left(-\frac{1}{15.0}\left(-\frac{C_{3d} - 10}{15.0}\right)\right) \tag{9}$$

in which $C_{3d}$ is expressed in centimeters. Only the snowfalls exceeding 10 cm were taken into account in this computation. Figure 3 shows the empirical probability distribution of $C_{3d}$ in a log linear diagram and the fitted exponential distribution. We also determined the maximum annual three-day snowfall: $C_{3d} = 47.5 - 18.6 \ln(-\ln(1 - T^{-1}))$ (expressed in centimeters) where $T = 1/(1 - P_C)$ is the

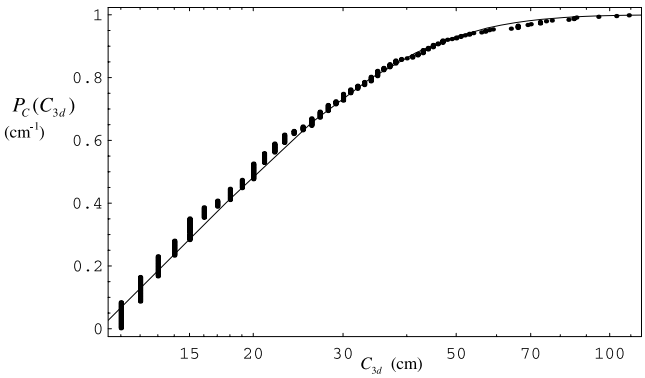


**Figure 3.** Empirical cumulative probability distribution of three-day sum of snowfall in Chamonix (France).

return period of snowfall ($P_C = \int p_C dC$), expressed in years. Assuming that the three-day sum of new snow is the main explanatory variable in the avalanche release, we have matched the meteorological and the avalanche databases to evaluate $p(\text{release}|C_{3d})$. Using logistic regression techniques [*Hosmer and Lemeshow*, 1986], we found that for $C_{3d} > 0$:

$$p(\text{release}|C_{3d}) = \frac{\exp(-4.0362 + 0.053C_{3d})}{(1 + \exp(-4.0362 + 0.053C_{3d}))} \quad (10)$$

The Hosmer-Lemeshow adjustment test provides a score of 0.5528 while the Pearson test gives a score of 0.9574. Both tests indicate the reliability of this model to evaluate $p(\text{release}|C_{3d})$. Further computations were performed with other explanatory variables (snow fallen during the preceding 24 h, mean wind intensity, maximal temperature of the air, etc.). We found that the most meaningful variable was the three-day sum of snow when a single variable was used.

[30] The second site is above Bessans (Maurienne Valley). The path extends between 3150 and 1700 m in elevation for a total length exceeding 2.1 km. The cross section is very irregular: the middle part of the path is confined in a steep and curly gully while both the starting zone and the deposition are wide unconfined surfaces. Since 1901, 127 avalanches have been documented. Figure 4 reports the empirical cumulative distribution function of the runout distance together with the path slope profile. The meteorological station (1710 m), 2.5 km from the starting zone, has been recording snow data since 1981. Using the renewal method, we have found that the probability of observing a snowfall $C_{3d}$ over three days is:

$$p_C(C_{3d}) = \exp\left(-\frac{1}{17.95}\frac{C_{3d} - 47.5}{18.6}\right) \quad (11)$$

The maximum three-day snowfall is described by: $C_{3d} = 47.5 - 18.6 \ln(-\ln(1 - T^{-1}))$ ($C_{3d}$ expressed in centimeters, $T$ in years). The release probability was found to be:

$$p(\text{release}|C_{3d}) = \frac{\exp(-4.0065 + 0.038C_{3d})}{(1 + \exp(-4.0065 + 0.038C_{3d}))} \quad (12)$$

The Hosmer-Lemeshow test yields 0.5594 while the Pearson test provides 0.9505.

### 3.4. Estimation of the Runout Distance Function *Y*

[31] For field applications, we need to obtain a numerical estimate of the runout distance function: $x_{stop} = Y(\mu, C_{3d}; \xi)$. For this purpose we performed $N_s^2$ simulations using the VSG model. Typically we took $N_S = 150$. For each simulation, we varied the initial conditions $\mu$ and $C_{3d}$ in the ranges 0.05–0.7 and 0.2–4 m, respectively (with a uniform spacing), while the friction coefficient $\xi$ was kept constant. The simulated runout elevations were then interpolated by third-order polynomials and a numerical estimate of $J_x$ was obtained. In a similar way, we computed the inverse function $Y^{-1}$ ($x_{stop}$, $C_{3d}$; $\xi$). For both avalanche paths, we took $\xi = 800$ m/s$^2$. As exemplified in Figure 5 for the Plan de l'Aiguille site, the variations in the runout distance are mainly dictated by the value of the coefficient $\mu$; the coefficient $\xi$ affects the runout distance to a lesser extent.

### 3.5. Direct Inversion

[32] For the period for which the meteorological stations have been in operation, it is possible to directly find the values of the coefficient $\mu$ for each avalanche run recorded in the database. For each event, we sought the amount of snow fallen over the previous three days $C_{3d}$ in the meteorological database. When this quantity was nonzero,

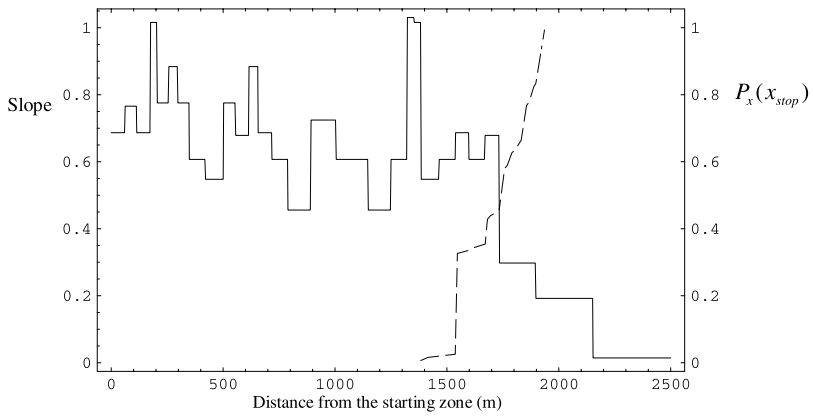


**Figure 4.** Variation in the path slope as a function of the distance from the starting point (solid line) along with the cumulative distribution function of the runout distance for the Bessans site.

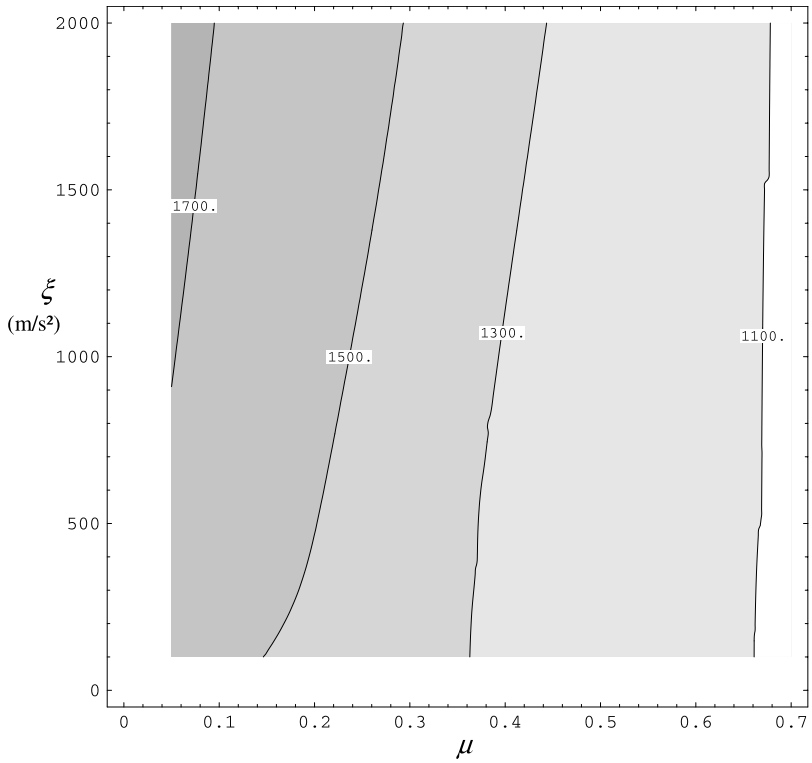


**Figure 5.** Contour plot of the runout distance as a function of $\mu$ and $\xi$ for $C_{3d}$ = 1 m in the case of the Plan de l'Aiguille site.

we computed the value $\mu$: $Y^{-1}$ ($x_{stop}$, $C_{3d}$; $\xi$). For the Plan de l'Aiguille site, 13 events were recorded over the period 1983–2001 and 9 were consecutive to snowfalls. For the Bessans site, 24 events were recorded over the period 1980–2001 and 21 events were consecutive to snowfalls. After deducing the $\mu$ values, we computed the cumulative distribution function of $\mu$. Figure 6 shows the typical results obtained for the Plan de l'Aiguille site. The distribution is not regular but step-shaped, with a first step at $\mu$ = 0.36 and a second step at $\mu$ = 0.56 (see Figure 9 for the complete histogram of $\mu$ values). This implies that the probability density function $p_\mu$ is not a uniformly varying function over the interval [0, 1], but on the contrary varies abruptly near the two values $\mu$ = 0.36 and $\mu$ = 0.56. A similar trend was obtained for the Bessans site, except that the peaks are located at $\mu$ = 0.31 and $\mu$ = 0.49 (see Figure 11).

[33] As mentioned above, there is substantial uncertainty on the runout distance and it is therefore necessary to

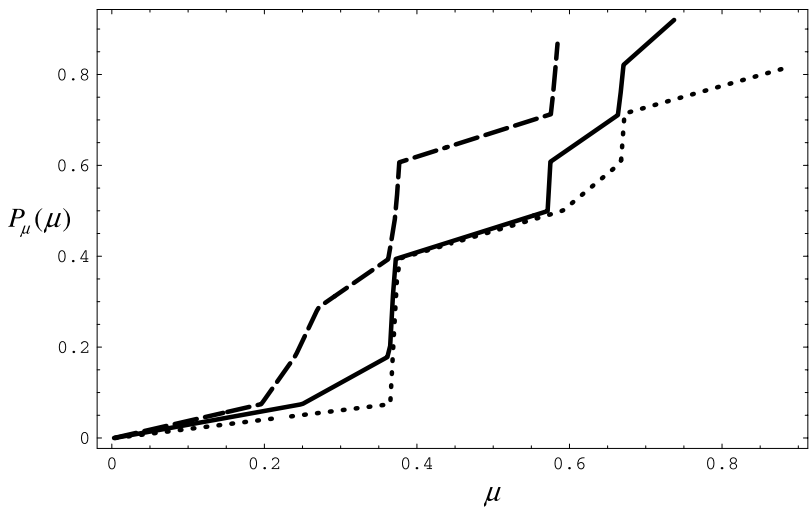


**Figure 6.** Empirical cumulative distribution function of the coefficient $\mu$ when it is assumed that there is no bias in the recorded runout distance (solid line), there is a systematic shift of 50 m (dashed line), or there is a systematic shift of −50 m (dotted line). Computations are for the Plan de l'Aiguille site and $\xi$ = 800 m/s$^2$.

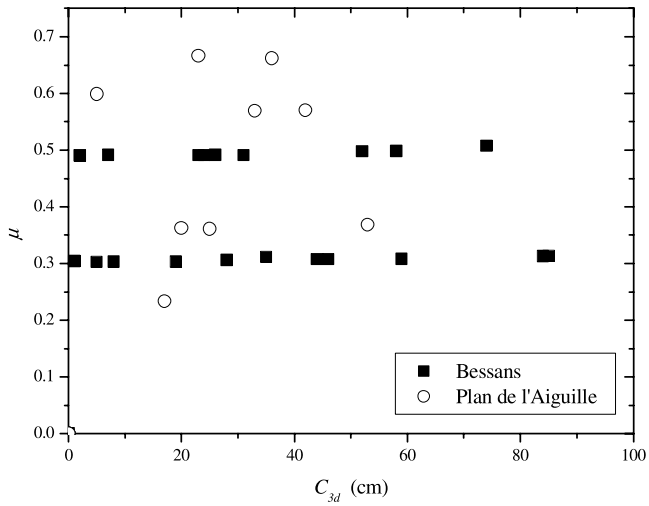


**Figure 7.** Variation of μ as a function of the three-day sum of snow for the two sites.

examine how this uncertainty affects the distribution of μ. A crude way of doing this is to assume that there was a systematic bias in the measurement of the runout distance. In this way we should obtain the upper and lower bounds of the range over which the coefficient μ varies. Figure 6 reports the results by assuming a systematic shift of −50 m or +50 m (±50 is the average uncertainty of the runout distance measurement). The first part of the empirical cumulative distribution (up to $\mu = 0.2$) has been drawn though it is likely that it is meaningless from a physical point of view. A bias of −50 m shifts the distribution of μ to the left without significantly altering the form of the distribution. A systematic decrease in the runout distance by +50 m smooths the distribution slightly, but it still rises strongly at $\mu = 0.36$ and $\mu = 0.56$. It follows that the structural features of the μ distribution depend a great deal on the uncertainty on the runout distance.

[34] Figure 7 shows the variation of the μ coefficient as a function of the three-day sum of snowfall for the Bessans and Plan de l'Aiguille sites. The points located at the axis origin represent the avalanches which were released, although there was no snowfall during the previous three days. No specific dependence of the μ coefficient on the snowfall was detected. At the Bessans site, data are not scattered but concentrate toward particular values, corresponding to the peak of the probability density function of μ. The same conclusion can be drawn from the Plan de l'Aiguille site (see Figure 7), but the concentration toward particular values is less pronounced. There is no clear explanation of this difference in behavior. When examining the path profiles (see Figures 2 and 4), it can be seen that for the Plan de l'Aiguille site the variations in the runout distance distribution are due to a significant decrease in the mean slope while the path slope influence is greatly attenuated for the Bessans site. Figure 7 raises a question on the reliability of the framework used for modeling the avalanche activity: it can be seen that many avalanches occurred as a result of small snowfalls. In fact, the reported values of snowfall do not really stand for the actual snowfalls over the starting zone since the meteorological stations are located more than 1000 m below the release zone.

[35] We have also checked that the results are not substantially influenced by the primary choice of the ξ value. Figure 8 shows the empirical probability density function of the μ coefficient for three different values of ξ in the case of the Plan de l'Aiguille site: ξ = 600, 800, and 1000 m/s$^2$. The deviation from one curve to another is low, demonstrating that for this path profile, the distribution of the μ coefficient is weakly dependent on the ξ coefficient. This is a helpful result in the present context: it shows that we can consider ξ as an independent parameter that we can adjust if we have information on the velocity reached by the avalanches at certain points of the path profile. Such a result could be expected since, in the cases treated here (see Figure 5), the runout distance is more sensitive to the coefficient μ than the coefficient ξ: $\partial Y/\partial\mu \gg \partial Y/\partial\xi$. It is unclear, however, if this result can be generalized to all avalanche paths.

### 3.6. Indirect Inversion

[36] To better understand the interest of the indirect method in the inversion problem, we proceeded in two

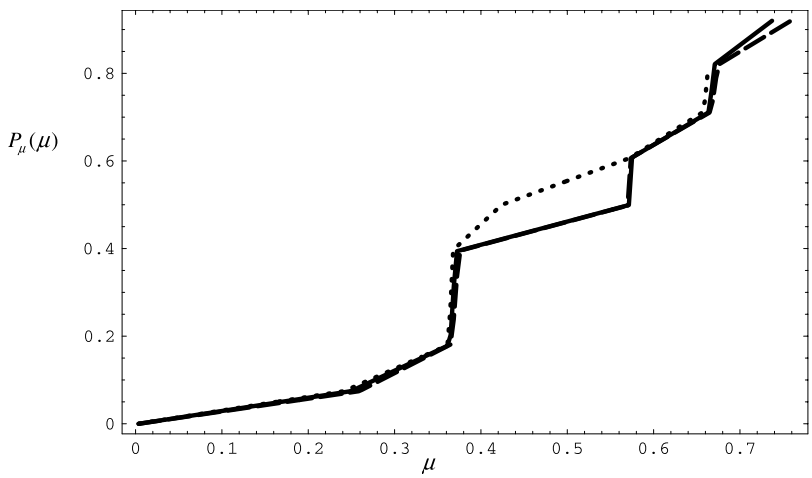


**Figure 8.** Empirical cumulative distribution function of the coefficient μ depending on the value of ξ: ξ = 800 m/s$^2$ (solid line), ξ = 1000 m/s$^2$ (dashed line), and ξ = 600 m/s$^2$ (dotted line). Computations are for the Plan de l'Aiguille site.

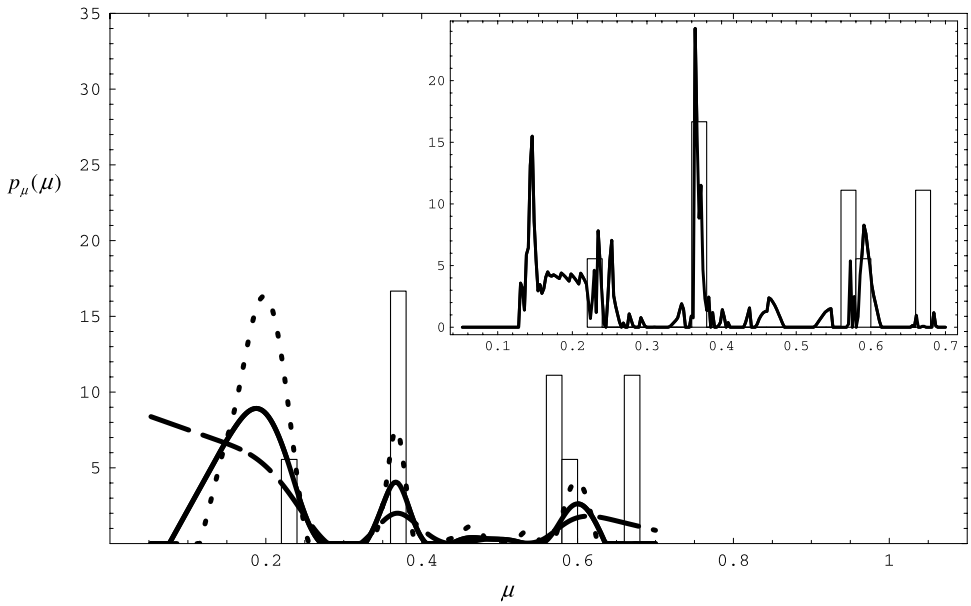


**Figure 9.** Empirical probability density function of the coefficient $\mu$ depending on the value of $\lambda$: $\lambda = 10^3$ (solid line, area = 1.29), $\lambda = 10^4$ (dashed line, area = 1.69), and $\lambda = 10^2$ (dotted line, area = 1.74). Computations are for the Plan de l'Aiguille site with $N_K = 250$ and $\mathbf{B} = \mathbf{L}_2$. The bars represent the scaled histogram of the $\mu$ values deduced from the direct method. In the inlet we have reported the empirical probability density function of the coefficient when the regularization operator is $\mathbf{B} = \mathbf{I}_{N_K}$. Computations are for the Plan de l'Aiguille site with $N_K = 250$ and $\lambda = 10^{-2.425}$ (area = 1.003).

steps. In the first step, we used the indirect method on the reduced data sample (corresponding to the period 1981–2001 for Bessans and 1960–2001 for Plan de l'Aiguille), as previously. This allowed us to test the method and compare it to the direct method. In the second step, we used all the data contained in the avalanche database.

[37] For the first step, in Figure 9 we have reported the resulting $\mu$ probability density functions for three different values of the parameter $\lambda$ for the Plan de l'Aiguille site. When $\mu$ takes its value in [0, 1], the constraint $\int p_\mu d\mu = 1$ cannot be achieved but it can be approached. A correct choice for $\lambda$ turned out to be $\lambda \approx 10^3$; we found $\int p_\mu d\mu = 1.29$. As apparent in Figure 9 and explained in section 2.3, the greater the value of $\lambda$, the smoother the resulting curve. In the same figure, we have drawn the histogram of the $\mu$ values deduced using the direct inversion (same data as in Figure 6). A simple examination of Figure 9 shows that for the range of $\lambda$ values tested here the indirect method provides probability density functions of the $\mu$ coefficient that are fairly consistent with the results obtained using the direct method: the different peaks in the $\mu$ distribution are clearly identified, except the last one at $\mu = 0.66$. However, compared to previous results, the probability distribution function $p_\mu(\mu)$ is smoother than expected and the peak amplitude is not respected. This is probably a direct consequence of our choice of a large value for $\lambda$. We have also used $\lambda$ values lower than $10^1$, but the resulting curves were very noisy, with too many oscillations to provide clear information on the variations in the $\mu$ coefficient. In short, we can draw the following conclusion from this preliminary comparison of the two methods: the indirect method based on Tikhonov regularization provides results that are consistent with those deduced using the direct inversion method. However, as the empirical probability distribution function defines an irregular curve made up of four peaks, the indirect method does not capture the features of this curve fully: to reduce the noise, we are forced to select large values of the $\lambda$ parameter; but, at times, this choice involves smoothing out the rapid variations in the $\mu$ coefficient. The fairly good agreement between the two methods may be somewhat surprising in that it has been stated that not all the avalanches of the database were consecutive to snowfalls. Thus the direct method dealt with avalanches released after snowfalls (9 events out of 13 for the Plan de l'Aiguille, that is, 69% of the recorded events), while in the indirect method such discrimination was neither possible nor reflected in the release probability $p(\text{release}|C_{3d})$; indeed, in the latter case, extrapolating equation (10) to $C_{3d} = 0$ provides a release probability $p(\text{release}|C_{3d} = 0) = 1.8\%$, far lower than the value empirically found (31%).

[38] For the second step, in Figure 10 we have reported the resulting probability density function of the coefficient $\mu$ for the Plan de l'Aiguille site: the dashed line represents the curve obtained with the full set of runout distances while the solid lined stands for the reduced set (same curve as in Figure 9). The inset in Figure 10 shows the sensitivity of $p_\mu(\mu)$ to changes in the $\lambda$ value by reporting the $\mu$ probability density functions obtained for $\lambda = 10$, 242, and $10^4$. The value $\lambda = 242$ is the one for which the constraint $\int p_\mu d\mu = 1$ is fulfilled. For Figure 10, comparing the curves obtained by using the full and the reduced sets of runout distances reveals the very similar behavior of the two resulting curves. The differences between the curves mainly concern the amplitude of the first peak (at $\mu \approx 0.2$), which is significantly reduced, and the number of peaks (7 against 4 found previously).

[39] The same exercise was repeated with the Bessans data. The same trend as above was also observed for the

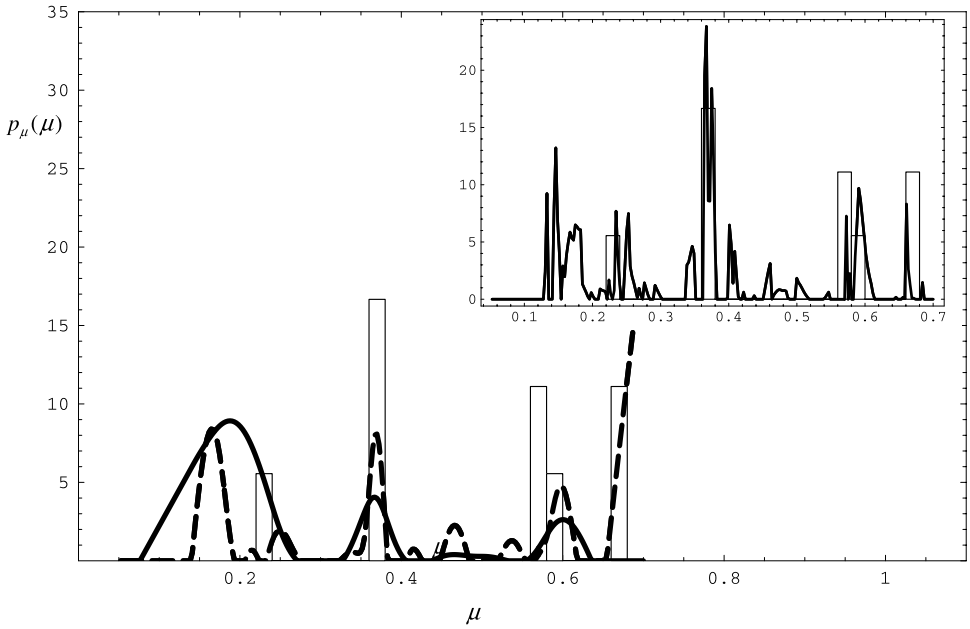


**Figure 10.** Empirical probability density function of the coefficient $\mu$ when the entire avalanche database is considered (dashed line, area = 1.02, $\lambda = 242$) or when only the recent avalanches (period 1983–2001) are taken into account (solid line, area = 1.29, $\lambda = 10^3$). Computations are for the Plan de l'Aiguille site and with $N_K = 250$. In the inset we have reported the empirical probability density functions of the coefficient $\mu$ when the entire avalanche database is considered and the regularization operator is $\mathbf{B} = \mathbf{I}_{N_K}$. Computations are for the Plan de l'Aiguille site with $N_K = 250$ and $\lambda = 10^{-2.5}$ (area = 0.999).

Bessans site except it was impossible to fulfill, even roughly, the constraint $\int p_\mu d\mu = 1$. We found no clear explanation for this odd behavior of the Bessans data.

### 3.7. Discussion

[40] The direct inversion method provides accurate estimates of the $\mu$ probability density function. However, this requires working with both the meteorological and avalanche databases. Since in most cases the period covered by the meteorological database is limited (to typically two decades, sometimes three or four decades), it is not certain that rare extreme events are included in the avalanche database. Thus, probably, this method provides partial information on the $\mu$ probability density function and underestimates the value of $\mu$ for extreme avalanches. Typically we found that the lowest values of $\mu$ were 0.24 for the Plan de l'Aiguille and 0.30 for Bessans; both values were larger than the typical values ($\mu \approx 0.155$) given in the literature [*Buser and Frutiger*, 1980].

[41] In the indirect inversion method, the time series of snowfall is replaced by the probability distribution of snowfall. This method can be used over the entire period covered by the avalanche database (typically a century for the avalanche paths investigated here). Since it is based on a denoising process (Tikhonov regularization), it slightly smooths out the rapid variations in the friction coefficient $\mu$. Moreover, the general properties of a probability density function (positive, normalized) are not automatically taken into account as further constraints in the primary formulation of the problem. In general, it was not possible to meet the three following conditions at the same time: $p_\mu$ solution to equation (4), $\int_{\mathbb{R}_+} p_\mu d\mu = 1$, and $p_\mu \geq 0$. A proper choice of the parameter $\lambda$ usually, but not always, allowed us to find a solution fulfilling the first two conditions while the third was imposed artificially by removing negative values. This is probably the greatest drawback of the numerical method implemented here for solving the Fredholm equation (equation 3): the curve sought is constrained to be smooth to a more or less large extent (controlled by the value given to $\lambda$) while, obviously, the solution curve is not smooth over the entire range of possible values for $\mu$. Though the indirect inversion method does not provide the exact probability density function of $\mu$, it can be used to locate the position of the peak values.

[42] Both methods have shown that the $\mu$ probability density function is not a slowly varying function but, on the contrary, defines a rapidly varying curve, made up of two or more peaks. It has also been shown that the coefficient $\mu$ is likely to be independent of the amount of snowfall preceding the avalanche release. These results contrast with the usual assumptions made on the $\mu$ variations. Indeed, in the primary formulation of the VSG model [*Salm et al.*, 1990], the $\mu$ coefficient is expected to be volume-dependent, that is, it should depend on the three-day sum of snowfall. However, Figure 7 reveals no relationship between $\mu$ and $C_{3d}$. Other formulations [e.g., *Barbolini and Savi*, 2001; *Bozhinskiy et al.*, 2001] have admitted that the probability density function of $\mu$ is a regularly increasing function. This assumption is not supported by the results in Figures 9–11. On the contrary, the present work demonstrates that, in a VSG-like model, the coefficient $\mu$ is a discrete random variable rather than a continuous random variable.

[43] Furthermore, the two investigated sites provide the same overall features in the $\mu$ distribution even though the

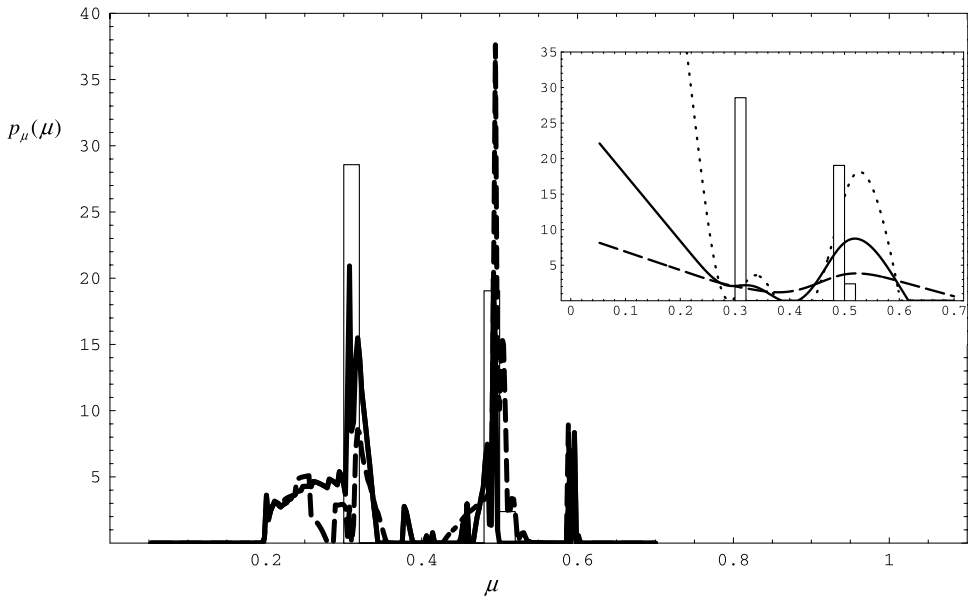


**Figure 11.** Empirical probability density function (dashed line) of the coefficient μ when all the events of the avalanche database are considered (area = 1.00). The solid line stands for the probability density function evaluated using the indirect inversion method applied to the reduced set of runout distances. Computations are for the Bessans site, with $N_K = 250$, $\mathbf{B} = \mathbf{I}_{N_K}$, and $\lambda = 10^{-2.63}$. In the inset we have reported the probability density function of the coefficient μ when all the events of the avalanche database are considered and for different values of λ: $\lambda = 10^4$ (solid line, area = 3.82), $\lambda = 10^3$ (dotted line, area = 16.82), and $\lambda = 10^5$ (dashed line, area = 1.54). Computations are for the Bessans site with $N_K = 250$ and **B** is the second-order difference operator.

two curves do not coincide; notably the μ values corresponding to the peaks of $p_\mu$ differ substantially from one site to another. At this stage, our results do not support the assumption made in the VSG model according to which the friction coefficient μ is a general parameter independent of the site. Further investigations are needed to elucidate this point. Compared to other inversion methods (e.g., Bayesian approaches), the methods presented here limit the amount of a priori information on the system parameters since only one parameter remains unevaluated (the friction coefficient ξ). However, they do not cope with uncertainty in the runout distance distribution. This is probably the major drawback of these two methods since the μ probability density function is affected to a varying extent by the uncertainty on $x_{stop}$. When discussing the intrinsic nature of the coefficient μ, it will be necessary to determine whether the disparities in the μ distributions at different sites reflect the uncertainty of the runout distance or a regional effect.

## 4. Conclusion

[44] In this paper, we have compared two methods for solving the inverse problem for the VSG avalanche dynamics model (i.e., finding the friction coefficient μ). The direct inversion method involves finding μ by directly solving the nonlinear equation: $x_{stop} = Y(\mu, C_{3d}; \xi)$ where $x_{stop}$ is the runout distance, $C_{3d}$ is the amount of snow fallen during the previous three days, ξ is another friction coefficient expected to be constant. To solve this equation, both the avalanche and meteorological databases must be used. The μ probability density function is then inferred from the resulting solutions to this equation computed for each event recorded in the avalanche database.

[45] The indirect method does not solve this equation directly but considers a variant form: if $x_{stop}$, $C_{3d}$, and μ are three random variables, linked together by the relationship $x_{stop} = Y(\mu, C_{3d}; \xi)$, then their probability density functions are also linked together. The indirect method uses this relationship for computing the μ probability density function.

[46] Both methods give similar results. The direct method is conceptually simpler and easier to implement numerically. The computer time is fairly low and the accuracy of the results is high. However, it requires using both the avalanche and meteorological databases. Consequently, it can be applied only to sites with a nearby meteorological station, whose records cover a sufficiently long period. In contrast, the indirect method is more complicated. Final results depend to a varying extent on the choice of the denoising process (Tikhonov regularization), the accuracy in the numerical estimation of different functions involved in the computations, etc. However, it has the great advantage of handling probability density functions rather than time series of events. Thus it can be easily applied to avalanche paths for which only the avalanche database covers a very long period. Both methods have shown that, contrary to many statements in the literature, the friction coefficient μ is likely to be independent of the amount of snow fallen during the days preceding the avalanche release. Moreover, the coefficient μ can be approximated as a discrete random variable.

[47] Further investigations are under way to improve the numerical implementation of the method and its robustness and to test it to different series of close avalanche paths.

[48] **Acknowledgments.** This study was supported by the Ministère de l'Environnement et de l'Aménagement du territoire (DPPR-MATE 2000 05 9 034 U). The authors are grateful to Eric Martin from Météo-France for providing snow data.

## References

Ancey, C., *Guide Neige et Avalanches: Connaissances, Pratiques, Sécurité*, Edisud, Aix-en-Provence, France, 1996.

Ancey, C., Snow avalanches, in *Geomorphological Fluid Mechanics: Selected Topics in Geological and Geomorphological Fluid Mechanics*, edited by N. J. Balmforth and A. Provenzalle, pp. 319–338, Springer-Verlag, New York, 2001.

Andreotti, B., and S. Douady, On probability distribution functions in turbulence. part 1. A regularisation method to improve the estimate of a PDF from an experimental histogram, *Physica D*, *132*, 111–132, 1999.

Baker, C. T. H., A perspective on the numerical treatment of Volterra equations, *J. Comput. Appl. Math.*, *125*, 217–249, 2000.

Bakkehøi, S., U. Domaas, and K. Lied, Calculation of snow avalanche run out distance, *Ann. Glaciol.*, *4*, 24–30, 1983.

Barbolini, M., and F. Savi, Estimate of uncertainties in avalanche hazard mapping, *Ann. Glaciol.*, *32*, 299–305, 2001.

Barbolini, M., U. Gruber, C. J. Keylock, M. Naaim, and F. Savi, Application of statistical and hydraulic-continuum dense-snow avalanche models to five European sites, *Cold Reg. Sci. Technol.*, *31*, 133–149, 2000.

Bartelt, P., and U. Gruber, Development and calibration of a Voellmy-fluid dense snow avalanche model based on a finite element method, *Rep. 714*, Eigd. Inst. für Schnee- und Lawinenforschung, Davos, Switzerland, 1997.

Bartelt, P., B. Salm, and U. Gruber, Calculating dense-snow avalanche runout using a Voellmy-fluid model with active/passive longitudinal straining, *J. Glaciol.*, *45*, 242–254, 1999.

Bozhinskiy, A. N., A. N. Nazarov, and P. A. Chernouss, Avalanches: A probabilistic approach to modelling, *Ann. Glaciol.*, *32*, 255–258, 2001.

Burkard, A., and B. Salm, Die Bestimmung der mittleren Anrissmächtigkeit $d_0$ zur Berechnung von Fliesslawinen, *Rep. 668*, Eigd, Institut für Schnee- und Lawinenforschung, Davos, Switzerland, 1992.

Buser, O., and H. Frutiger, Observed maximum run-out distance of snow avalanches and determination of the friction coefficients $\mu$ et $\xi$, *J. Glaciol.*, *26*, 121–130, 1980.

Calvetti, D., S. Morigi, L. Reichel, and F. Sgallari, Tikhonov regularization and the L-curve for large discrete ill-posed problems, *J. Comput. Appl. Math.*, *123*, 423–446, 2000.

Chernouss, P. A., and Y. Fedorenko, Application of statistical simulation for avalanche-risk evaluation, *Ann. Glaciol.*, *32*, 182–186, 2001.

Dent, J. D., and T. E. Lang, Modelling of snow flow, *J. Glaciol.*, *26*, 131–140, 1980.

Dent, J. D., and T. E. Lang, Experiments on the mechanics of flowing snow, *Cold Reg. Sci. Technol.*, *5*, 243–248, 1982.

Eglit, E. M., Some mathematical models of snow avalanches, in *Advances in the Mechanics and the Flow of Granular Materials*, edited by M. Shahinpoor, pp. 577–588, Trans Tech, Clausthal-Zellerfeld, Germany, 1983.

Eglit, M., Mathematical modeling of dense avalanches, in *25 Years of Snow Avalanche Research*, edited by E. Hestnes, pp. 15–18, Norw. Geotech. Inst., Voss, 1998.

Eglit, M. E., Theoretical approaches to avalanche dynamics, in *Soviet Avalanche Research and Avalanche Bibliography Update: 1977–1983*, *Glaciol. Data Report GD-16*, translated from Russian, pp. 63–117, U.S. Dep. of Agric. For. Serv., Washington, D. C., 1984.

Fujizawa, K., R. Tsunaki, and I. Kamishii, Estimating snow avalanche run-out distances from topographic data, *Ann. Glaciol.*, *18*, 239–244, 1993.

Ghali, A., Méthodes statistiques pour la détermination de la distance d'arrêt des avalanches, Ph.D. thesis, Univ. Joseph Fourier, Grenoble, France, 1996.

Gumbel, E. J., *Statistics of Extremes*, Columbia Univ. Press, New York, 1958.

Harbitz, C., A. Harbitz, and F. Nadim, On probability analysis in snow avalanche hazard zoning, *Ann. Glaciol.*, *32*, 290–298, 2001.

Hopf, J., An overview of natural hazard zoning with special reference to avalanches, in *25 Years of Snow Avalanche Research*, edited by E. Hestnes, pp. 28–35, Norw. Geotech. Inst., Voss, 1998.

Hopfinger, E. J., Snow avalanche motion and related phenomena, *Annu. Rev. Fluid Mech.*, *15*, 45–76, 1983.

Hosmer, D. W., and S. Lemeshow, *Applied Logistic Regression*, Wiley-Interscience, New York, 1986.

Hunt, B., Newtonian fluid mechanics treatment of debris flows and avalanches, *J. Hydraul. Eng.*, *120*, 1350–1363, 1994.

Hutter, K., Avalanche dynamics, in *Hydrology of Disasters*, edited by V. P. Singh, pp. 317–392, Kluwer Acad., Norwell, Mass., 1996.

Keylock, C. J., and M. Barbolini, Snow avalanche impact pressure—Vulnerability relations for use in risk assessment, *Can. Geotech. J.*, *38*, 227–238, 2001.

Keylock, C. J., D. M. McClung, and M. M. Magnússon, Avalanche risk mapping by simulation, *J. Glaciol.*, *45*, 303–314, 1999.

Kirsch, A., *An Introduction to the Mathematical Theory of Inverse Problems*, Springer-Verlag, New York, 1996.

Lied, K., and S. Bakkehøi, Empirical calculations of snow avalanche run-out distances based on topographic parameters, *J. Glaciol.*, *26*, 165–177, 1980.

McClung, D. M., Extreme avalanche runout in space and time, *Can. Geotech. J.*, *37*, 161–170, 2000.

McClung, D. M., Extreme avalanche runout: A comparison of empirical models, *Can. Geotech. J.*, *38*, 1254–1265, 2001.

McClung, D. M., and K. Lied, Statistical and geometrical definition of snow avalanche runout, *Cold Reg. Sci. Technol.*, *13*, 107–119, 1987.

McClung, D. M., and A. I. Mears, Dry-flowing avalanche run-up and run-out, *J. Glaciol.*, *41*, 359–372, 1995.

McClung, D. M., and P. A. Schaerer, *The Avalanche Handbook*, The Mountaineers, Seattle, Wash., 1993.

Mears, A. I., Snow-avalanche hazard analysis for land-use planning and Engineering, *Bull. 49*, Colo. Geol. Surv., Denver, 1992.

Norem, H. F., F. Irgens, and B. Schieldrop, A continuum model for calculating snow avalanche velocities, in *Symposium on Avalanche Formation, Movement and Effects*, *IAHS Publ.*, *186*, 363–379, 1986.

Press, W. H., S. A. Teukolsky, W. T. Vetterling, and B. P. Flannery, *Numerical Recipes in Fortran: The Art of Scientific Computing*, Cambridge Univ. Press, New York, 1992.

Salm, B., Flow, flow transition and runout distances of flowing avalanches, *Ann. Glaciol.*, *18*, 221–226, 1993.

Salm, B., A. Burkard, and H. Gubler, Berechnung von Fliesslawinen, eine Anleitung für Praktiker mit Beispielen, *Rep. 47*, Eigd. Inst. für Schnee- und Lawinenforschung, Davos, Switzerland, 1990.

Savage, S. B., Flow of granular materials, in *Theoretical and Applied Mechanics*, edited by P. Germain, J.-M. Piau, and D. Caillerie, pp. 241–266, Elsevier Sci., New York, 1989.

Savage, S. B., and K. Hutter, The motion of a finite mass of granular material down a rough incline, *J. Fluid Mech.*, *199*, 177–215, 1989.

Schaerer, P. A., Friction coefficients and speed of flowing avalanches, in *Symposium Mécanique de la Neige*, *IAHS Publ.*, *114*, 425–432, 1974.

Tai, Y.-C., K. Hutter, and J. M. N. T. Gray, Dense granular avalanches: Mathematical description and experimental validation, in *Geomorphological Fluid Mechanics: Selected Topics in Geological and Geomorphological Fluid Mechanics*, edited by N. J. Balmforth and A. Provenzalle, pp. 339–366, Springer-Verlag, New York, 2001.

C. Ancey, M. Meunier, and D. Richard, Research Unit Torrential Erosion, Snow and Avalanches, Domaine Universitaire, 38402 Saint-Martin-d'Hères Cedex, France. (christophe.ancey@cemagref.fr)